Available online at www.sciencedirect.com
ScienceDirect
Journal of Molecular Graphics and Modelling 25 (2006) 17–29
Journal of Molecular Graphics and Modelling
www.elsevier.com/locate/JMGM

A putative bioactive conformation for the altered peptide ligand of myelin basic protein and inhibitor of experimental autoimmune encephalomyelitis [Arg^{91}, Ala^{96}] MBP$_{87–99}$

E.D. Mantzourani [a,b], T.V. Tselios [b], S. Golič Grdadolnik [c], A. Brancale [d], J.A. Platts [e], J.M. Matsoukas [b], T.M. Mavromoustakos [a,*]

[a] *National Hellenic Research Foundation, Institute of Organic and Pharmaceutical Chemistry, 48 Vassileos Constantinou Avenue, 116 35 Athens, Greece*
[b] *University of Patras, Department of Chemistry, 265 00 Rion, Patras, Greece*
[c] *Laboratory for Molecular Modeling and NMR Spectroscopy, National Institute of Chemistry, Hajdrihova 19, SI-1001 Ljubljana, Slovenia*
[d] *Welsh School of Pharmacy, Cardiff University, Redwood Building, King Edward VII Avenue, CF1 3XF Cardiff, Wales, UK*
[e] *Department of Chemistry, Cardiff University, P.O. Box 912, CF10 3TB Cardiff, Wales, UK*

Received 14 June 2005; received in revised form 22 September 2005; accepted 29 September 2005
Available online 28 November 2005

Abstract

[Arg^{91}, Ala^{96}] MBP$_{87–99}$ is an altered peptide ligand (APL) of myelin basic protein (MBP), shown to actively inhibit experimental autoimmune encephalomyelitis (EAE), which is studied as a model of multiple sclerosis (MS). The APL has been rationally designed by substituting two of the critical residues for recognition by the T-cell receptor. A conformational analysis of the APL has been sought using a combination of 2D NOESY nuclear magnetic resonance (NMR) experiments and detailed molecular dynamics (MD) calculations, in order to comprehend the stereoelectronic requirements for antagonistic activity, and to propose a putative bioactive conformation based on spatial proximities of the native peptide in the crystal structure. The proposed structure presents backbone similarity with the native peptide especially at the N-terminus, which is important for major histocompatibility complex (MHC) binding. Primary (Val^{87}, Phe^{90}) and secondary (Asn^{92}, Ile^{93}, Thr^{95}) MHC anchors occupy the same region in space, whereas T-cell receptor (TCR) contacts (His^{88}, Phe^{89}) have different orientation between the two structures. A possible explanation, thus, of the antagonistic activity of the APL is that it binds to MHC, preventing the binding of myelin epitopes, but it fails to activate the TCR and hence to trigger the immunologic response. NMR experiments coupled with theoretical calculations are found to be in agreement with X-ray crystallography data and open an avenue for the design and synthesis of novel peptide restricted analogues as well as peptide mimetics that rises as an ultimate goal.

Keywords: [Arg^{91}, Ala^{96}] MBP$_{87–99}$; Bioactive conformation; NMR; Molecular dynamics; Major histocompatibility complex; T-cell receptor

1. Introduction

Multiple sclerosis (MS) is an inflammatory, demyelinating disease involving the white matter of the central nervous system (CNS), prevalent in Northern Europeans and North Americans. As the name of the disease implies, affected individuals exhibit hardened (or ''sclerotic'') tissue in many (or ''multiple'') parts of brain and spinal cord [1]. It affects mostly young and middle-aged adults leading to substantial disability in more than 50% of the patients [2]. Its etiology remains unknown, but both environmental and genetic factors seem to govern the generation of the disease. Previous studies have demonstrated that the HLA-DR2b (DRB1*1501) haplotype is present at an increased frequency in northern European Caucasoid patients with MS [3,4]. Genes of the major histocompatibility complex (MHC) class II region are the only ones that have been consistently associated with the disease. However, susceptibility is probably mediated by a heterogeneous array of genes [2]. The composition of demyelinated MS plagues, immunogenetic background, response to immunodulatory and immunosuppressive therapy, and data from animal models support

* Corresponding author.

1093-3263/$ – see front matter © 2005 Elsevier Inc. All rights reserved.
doi:10.1016/j.jmgm.2005.09.010

that MS is an autoimmune disease mediated by neuroantigen myelin-specific CD4 T cells. Candidate autoantigens include constituents of the myelin sheath such as myelin basic protein (MBP) and proteolipid protein (PLP); the antigenic components of myelin in MS, though, have not been identified with certainty yet. The current and emerging therapies available for MS are non-specific, may have toxic side effects or cannot be used in long-term treatment [5–9]. Therefore, antigen-specific therapeutic approaches that suppress autoreactive T cells are nowadays preferred.

Experimental autoimmune encephalomyelitis (EAE), the best animal model for MS, is a relapsing experimental demyelinating disease, characterized by focal areas of inflammation and demyelination throughout the CNS. EAE is induced by injection of large doses of the referred myelin antigens, in a soluble form [10]. Modern approaches towards the therapeutic management of MS involve the design and use of peptide analogues of disease-associated myelin epitopes. The idea is to block the formation of the trimolecular complex MHC–altered peptide ligand (APL)–T-cell receptor (TCR) and therefore to interrupt the process of the disease [11]. Considerable work has been done in this area [12–14,20] but phase II clinical trials have been suspended [15,16] due to hypersensitivity reactions in a percentage of the patients. This addresses the need for more refined work on the elimination of the potential limitation of the approach.

A new line as an attempt to synthesize a stable molecule for clinical purposes while retaining the same biological activity, was the introduction of the more resistant towards proteolytic hydrolysis cyclic peptides. In previous studies based on the immunodominant human MBP epitope 87–99, we have shown that two antagonist cyclic analogues of $MBP_{87–99}$ are as effective as their linear counterparts, but more stable and selective. The specific epitope was chosen as it is a strong immunodominant epitope, and a number of APLs have been shown to inhibit EAE induced by guinea pig $MBP_{72–85}$ epitope [17].

Because linear peptides are a good starting point for intensive conformational studies and rational drug design, this work has been focused on an investigation of the 3D structure of such an APL, a linear EAE antagonist [Arg^{91}, Ala^{96}] $MBP_{87–99}$ [6,18] (Fig. 1) in which the amino acids Lys^{91} and Pro^{96} were replaced by Arg and Ala, respectively. The molecule has been rationally designed by substituting two of the critical residues for TCR recognition [19]. Lys^{91} and Pro^{96} are two anchor residues forming H-bonds with the TCR [20,21]. Moreover, Pro^{96} is possibly responsible for the formation of a bend and the subsequent shift of the remaining sequence so that it is accessible for contact with the TCR. The putative bioactive conformational of the synthetic APL is essential to understand better its physicochemical properties for antagonistic biological activity.

Within this context, a combination of unrestrained and backbone restrained molecular dynamics (MD) simulations, and experimental 1D and 2D nuclear magnetic resonance (NMR) spectroscopic methods has been applied to establish a

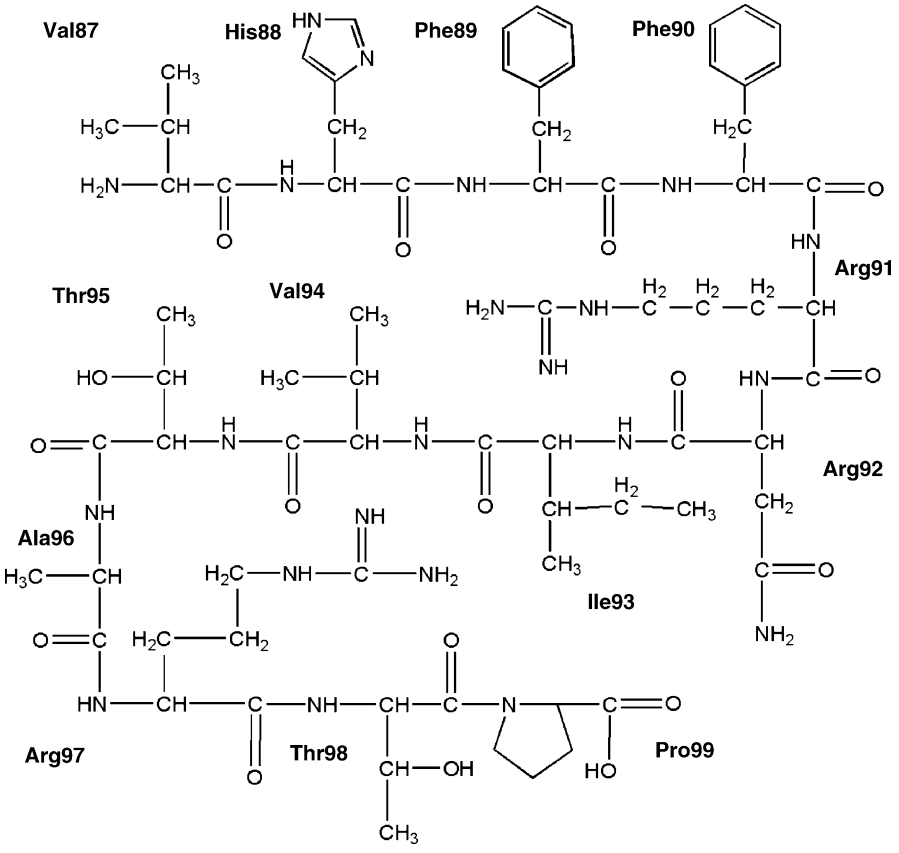

Fig. 1. Structure of the linear antagonist [Arg^{91}, Ala^{96}] $MBP_{87–99}$ under study.

putative bioactive conformation for the APL. This is defined as a conformation that enables binding with the MHC, but prevents binding with the TCR and therefore T-cell activation. The aim was not to calculate the average structure that complies with all NOEs and does not represent the real situation in solution, but instead, to shed light into the whole conformational ensemble. Such approach reveals many energetically favored conformations and agrees with the general accepted concept that peptides bind to their receptor in a low energy conformation, not necessarily the global minimum. The proposed bioactive conformation is indeed a low energy structure, in which a range of the experimental NOE distance restraints is in accordance with the conformation of $MBP_{85–99}$ provided by crystallographic data. This work establishes the necessity of using both experimental NOE data and theoretical modelling studies for exploring and understanding the stereo-electronic requirements for EAE inhibition in order to rationally design a peptide mimetic molecule.

2. Methodology

2.1. Synthesis of [Arg^{91}, Ala^{96}] $MBP_{87–99}$

Linear APL, [Arg^{91}, Ala^{96}] $MBP_{87–99}$, was synthesized step by step by Fmoc/tBu methodology using 2-chlorotrityl chloride (CLTR-Cl) resin (0.7 mmol Cl^-/g) and Na-Fmoc (9-fluorenylmethyloxycarboxyl)-protected amino acids as previously described [23]. The purification and identification of peptide were achieved using reverse phase-high performance liquid chromatography (RP-HPLC) and electron spray ionization (ESI) mass spectroscopy, respectively [17].

2.2. Nuclear magnetic resonance spectroscopy (NMR)

The high-resolution NMR spectra were recorded on a Varian INOVA 600-MHz spectrometer at 298 K. Five milligrams of peptide was dissolved in 0.7 ml of DMSO-d_6. The DQF-COSY [22], ^{1}H-^{13}C HSQC [23] and ^{1}H-^{13}C HSQC-TOCSY [24] experiments were performed with gradients. The TOCSY [25] and NOESY [26] experiments were recorded using standard pulse sequences in the phase-sensitive mode. Typically, the homonuclear proton spectra were acquired with a spectral width of 11371 Hz, 4096 data points in t_2, 16–32 scans, 324–412 complex points in t_1, and a relaxation delay of 1–1.5 s. The mixing time in NOESY and TOCSY experiments was 150 and 60 ms, respectively. Heteronuclear experiments were acquired with a ^{1}H spectral width of 6936 Hz, a ^{13}C spectral width of 20471 Hz, 1024 data points in t_2 and a relaxation delay of 1 s. The ^{1}H-^{13}C HSQC was recorded with 32 scans and 128 complex points in t_1. The ^{1}H-^{13}C HSQC-TOCSY was recorded with 128 scans, 256 complex points in t_1 and a mixing time of 32 ms.

Data were processed and analyzed with FELIX software package from Accelrys Software Inc. Spectra were zero-filled two times and apodized with a squared sine bell function shifted by $\pi/2$ in both dimensions. Cross-peak volumes in NOESY spectra were calculated by integration routine within the FELIX software. For calculation of distances the two-spin approximation was used and an integrated intensity of the geminal pair of protons γ_1 and γ_2 of Ile^{93} was assumed to have a distance of 1.78 Å. Based on these distances and direct observation of peaks, a set of strong (up to 2.8 Å), medium (2.8–3.8 Å), and weak (3.8–5.5 Å) NOEs was established.

2.3. Molecular modelling

Computer calculations were performed on a RM 3 GHz Pentium IV workstation using MOE 2004.03 by Chemical Computing Inc. [27]. Molecular dynamics simulations were performed and the derived conformations were examined for consistency with experimental distance information designated by the obtained NOEs. Thus, populations of various conformers that represent local minima at the potential energy surface are identified.

2.3.1. Generating the starting conformation

AMBER94 [28] force field was employed for all energy minimizations. An extended backbone structure of the peptide sequence was built, comprised of L-amino acids with standard parameters for all atom systems. As DMSO that was used in experimental studies is a polar, aprotic solvent, the side chain NH of Arg^{91} and Arg^{97} were set to an ionization state of zero. The structure of the linear antagonist was minimized using a succession of three methods: steepest descents (SD) algorithm to remove unfavorable steric contacts, then conjugate gradients to find its local minimum, followed by truncated Newton (TN). TN is the most efficient large scale non-linear optimization algorithm known. In all cases, energy convergence criterion is root mean square deviation (RMSD) force $\leq$0.001 kcal mol^{-1} $Å^{-1}$.

2.3.2. Molecular dynamics (MD) studies

Three sets of MD [29,30] runs were performed using AMBER94 force field. A dielectric constant of 45 was used, to simulate the DMSO environment. The MD production runs were performed with a time step of 0.002 ps employing Verlet's algorithm [31], for duration of 1 ns. An additional length of 100 ps heating time preceded the main simulation, to gradually heat the system from 1 to 298 K, for an effective simulation of the temperature of the NMR sample solution. Number of particles in the unit cell, volume, and temperature were chosen as the thermodynamic variables that were held constant. All bond lengths involving hydrogens or lone pairs were constrained.

The first set of dynamics was completely unrestrained (I) [32], using a sampling period of 5 ps. Two sets of backbone restrained dynamics were performed, using a sampling period of 2 ps. Backbone distance constraints were employed to allow enough freedom to the side chains, so that sufficient sampling of conformational space could be obtained. Upper and lower bounds were used to establish a target interval. A weight factor representing the force constant (in kcal/mol) of 50 was chosen, to determine the strength of the restraint relative to the total energy of the molecule. A value of 50 was found to allow substantial deviation from the target interval in order to obtain a

sufficient sampling, without raising significantly the total energy of the molecule.

Sequential NH–NH distance constraints were used in the first set (II), in an attempt to obtain conformations within the α_L region of the Ramachandran map [33], and sequential Hα-NH constraints were used in the second set (III), for sampling of the β region. All resulting conformations were subjected to a completely unrestrained energy minimization, following the same procedure described above, in order to make a direct comparison with the NMR results.

Selected structures had backbone dihedral angles φ and ψ within the core region of the Ramachandran map [34,35], and *trans* ω dihedral angles [36]. Virtual dihedral angle ζ was also examined, to evaluate the planarity of C_α.

The selected low energy structures were grouped into families according to their backbone dihedral angles and overall RMSD (in Å) when compared to the lowest energy structure of each run. For each cluster an RMSD of less than 1 Å was chosen. In some cases single conformations were classified as a cluster, provided they had a unique backbone conformation.

3. Results and discussion

3.1. Structure identification

The proton chemical shifts of [Arg^{91}, Ala^{96}] MBP$_{87–99}$ in the 1D ^{1}H NMR spectrum (Fig. 2) were assigned using 2D TOCSY and NOESY experiments in combination with 2D ^{1}H-^{13}C HSQC and 2D ^{1}H-^{13}C HSQC-TOCSY experiments (Supplementary data). Observed peaks are referenced to DMSO-d_6. For the assignment, the spin system of His^{88} was used as an initial pattern in TOCSY. Additional information was then used from the NOESY spectrum, in which sequential cross-peaks occur between $C_\alpha H_i$ and NH_{i+1} resonances ($d_{\alpha N(i,i+1)}$). The cross peak between the C_αH of the residue preceding the proline and the C_δH of the proline, was used to establish sequential assignment. This procedure allowed the establishment of backbone sequential connectivities for the entire peptide and thus make specific assignments for all the resonances, as summarized in Table 1.

The proton assignment, when compared with previously published results recorded on a 400-MHz spectrometer [37], is found to be in good agreement. The refinement of the assignment was considered necessary in order to clarify the NOE correlations that presented severe overlapping using lower resolution spectrometer. Indeed, different NOE connectivities were depicted due to the use of higher resolution 600 MHz spectrometer. Also, a thorough exploration of the conformational space of the peptide was sought.

Additionally, ^{13}C assignment was accomplished, in order to study the conformation of the proline peptide bond. One set of resonances was observed for [Arg^{91}, Ala^{96}] MBP$_{87–99}$ in DMSO-d_6, demonstrating the existence of a single conformation of the Thr^{98}–Pro^{99} peptide bond. Cβ of Pro^{99} was found to be at 28.5 ppm while Cγ was found at 24.2 ppm. The difference in ppm is 4.3, indicating that for the dominant conformers of the conformational ensemble the peptide bond of the Pro^{99} with Thr^{98} is *trans* and that *cis-trans* isomerization [38] does not occur. Powerful evidence for the *trans* nature of the peptide bond is provided by the NOE connectivities observed between γ Thr^{98} and δ_1 Pro^{99}, and β Thr^{98} and δ_2 Pro^{99}.

3.2. NOE connectivities

The proton-proton NOE connectivities were collected from the NOESY spectrum measured at 150 ms. The list of observed inter-residue NOE connectivities is presented in Table 2.

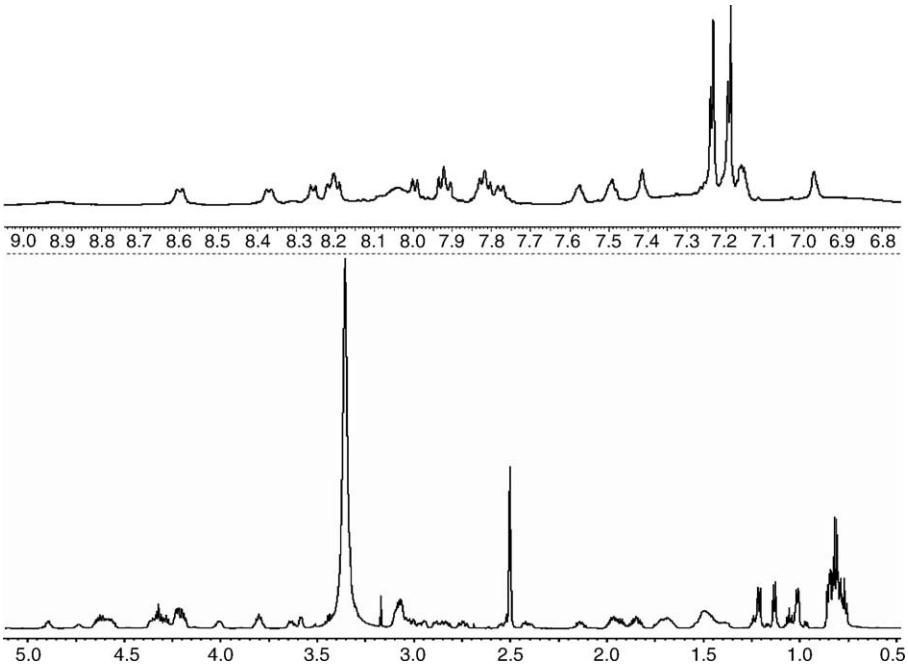

Fig. 2. ^{1}H NMR spectrum of [Arg^{91}, Ala^{96}] MBP$_{87–99}$ in DMSO-d_6 recorded on a Varian INOVA 600 MHz spectrometer.

Table 1
Assignment of the ^{1}H spectrum (top lines in the amino acid sequences), using as a reference DMSO at 2.49 ppm

Amino acids	NH	α	β	γ	δ	Other protons
Val[87]	8.03	3.58 56.8	1.96 29.8	0.81 18.1	–	
His[88]	8.59	4.63 51.0	β_1:2.94 β_2:2.87 27.2	–	–	2H:8.91, 133.4 4H:7.24, 126
Phe[89]	8.19	4.56 53.4	β_1:3.01 β_2:2.74 37.2	–	–	Ring:7.17 128.8, 127.6
Phe[90]	8.36	4.58 53.4	β_1:3.02 β_2:2.83 37.2	–	–	Ring:7.21 128.9, 127.6
Arg[91]	8.20	4.35 51.5	β_1:1.68 β_2:1.49 29.0	1.52 24.5	3.08 40.1	εNH: 7.57 38.6
Asn[92]	8.25	4.61 49.4	β_1:2.54 β_2:2.42 36.7	–	–	ε_1NH:6.97 ε_2NH: 7.41,
Ile[93]	7.76	4.22 56.6	1.71 36.4	γ_1:1.04, γ_2:1.38 23.7	0.78 10.7	$\gamma_{(CH3)}$: 0.79 15.0
Val[94]	7.90	4.20 57.9	1.95 29.8	0.85 18.9	–	–
Thr[95]	7.79	4.21 57.9	3.99 66.4	1.01 19.2	–	OH: 4.90
Ala[96]	7.81	4.27 47.8	1.21 17.9	–	–	–
Arg[97]	7.99	4.32 51.5	β_1:1.67 β_2:1.49 29.0	1.47 24.5	3.07 40.1	εNH: 7.49
Thr[98]	7.92	4.32 56.6	3.79 66.6	1.13 19.2		OH: 4.73
Pro[99]	–	4.20 57.9	β1:1.83 β2:2.14 28.5	γ_1: 1.92 γ_2: 1.85 24.2	δ1: 3.80 δ_2: 3.64 46.8	–

The ^{13}C assignment is also accomplished (bottom lines in amino acid sequences), using a combination of TOCSY, NOESY, ^{1}H-^{13}C HSQC and ^{1}H-^{13}C HSQC-TOCSY experiments, and DMSO-*d*6 at 39.5 ppm.

As with most short linear peptides in solution, the molecule is expected to be fluctuating over an ensemble of conformations with their φ and ψ angles lying within the broad minima of the conformational energy [39] diagram. Indeed, observation of extended regions of both sequential NOE connectivities $d_{\alpha N(i,i+1)}$ and $d_{NN(i,i+1)}$, indicate a conformational averaging between the α_R and β regions of φ, ψ space [40]. Consecutive $d_{NN(i,i+1)}$ peaks are observed between the NH proton resonances of all but Arg[91]–Asn[92], Val[94]–Thr[95], Thr[95]–Ala[96], and Arg[97]–Thr[98], which are overlapped with the main diagonal. The consecutive $d_{NN(i,i+1)}$ NOE connectivities cannot be indicative for the presence of populations with regular helical structure, because the $d_{\alpha N(i,i+3)}$ or $d_{\alpha\beta(i,i+3)}$ connectivities that are diagnostic of a regular helix are absent.

The strong sequential $d_{\alpha N(i,i+1)}$ along the entire backbone and absence of any long-range NOEs indicate the presence of a significant number of populations where [Arg[91], Ala[96]] $MBP_{87–99}$ adopts an extended conformation. However, observation of a number of medium-range NOEs at different parts of the peptide backbone identifies the presence of populations with segments of local folded structure in the conformational ensemble.

A clear medium-range inter-residue NOE connectivity is observed between Hα Asn[92] and NH Val[94]. The observation of this $d_{\alpha N(i,i+2)}$ connectivity confirms the presence of at least a threshold population of a folded structure with short-range order. This prompted us to look for a $d_{\beta N(i,i+2)}$ NOE, in order to check if a type II β turn could be designated in the above population. Indeed, a cross peak between $H\beta_1$ Asn[92]–NH Val[94] was found. The formation of this turn is also in accordance with the strong NH Ile[93]–NH Val[94] cross peak presented in Table 2.

A number of other medium-range inter-residue NOE connectivities are also observed, indicative of various populations with backbone bends formed. There are cross peaks between the proton resonances of Hγ Val[87]–NH Phe[89],

Table 2
Observed inter-residue cross peaks in the NOESY spectrum, and their intensities

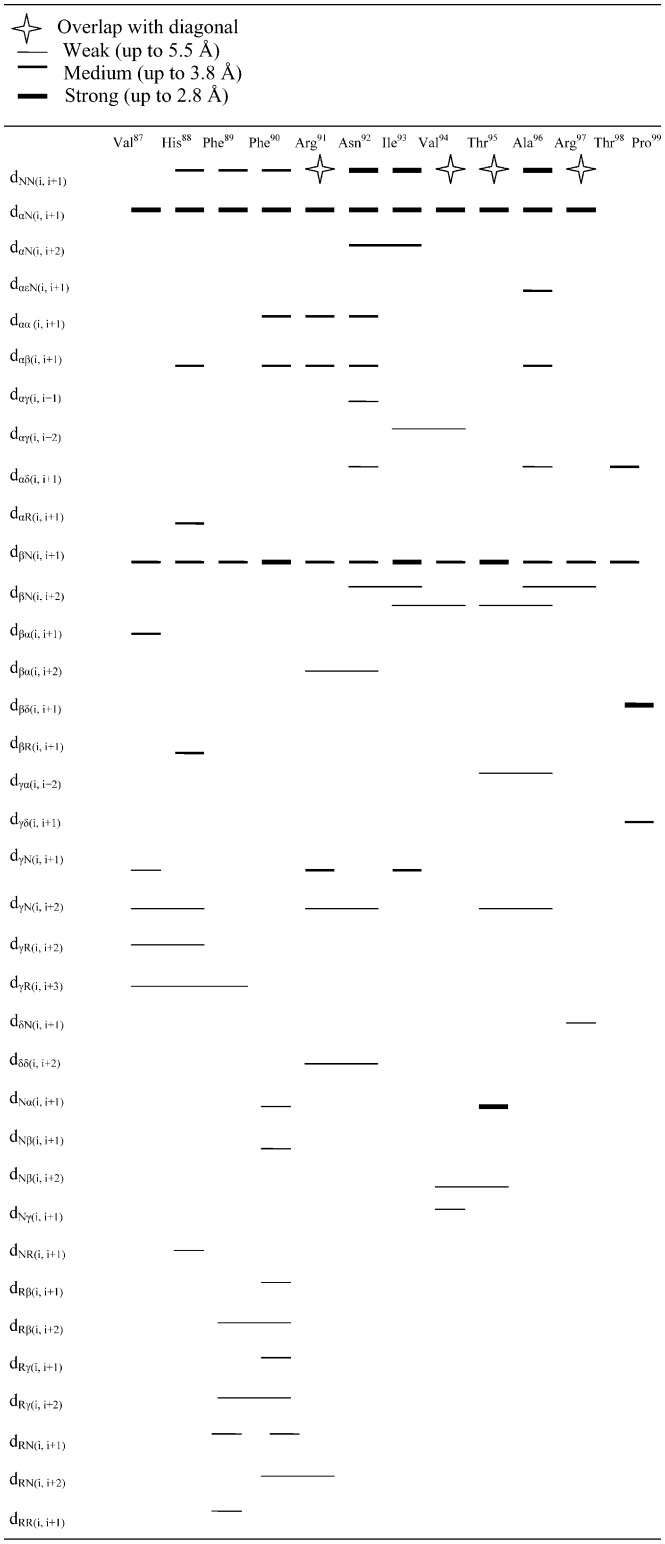

NH Phe[89]–Hβ$_1$ Arg[91], and Hβ Ala[96]–NH Thr[98]. For the interaction of Ile[93] with Thr[95] two NOE peaks are seen, Hβ Ile[93]–NH Thr[95], and Hα Ile[93]–Hγ Thr[95]. In the case of Val[94] and Ala[96] two medium-range connectivities are observed: in a moiety of the ensemble Hβ Ala[96] is in spatial proximity with Hγ Val[94] as well as NH Val[94]. More cross peaks are observed between Hγ$_{(CH3)}$ Ile[93] and Hβ$_2$ Arg[91] as well as Hδ Arg[91]. Hβ$_2$ Arg[91] also presents a cross peak with Hα Ile[93]. Cross peaks between Hγ Arg[91]–NH Ile[93], Hγ Thr[95]–Hα Arg[97], Hγ Thr[95]–NH Arg[97], and Hβ Thr[95]–NH Arg[97] were also observed.

3.3. MD simulations

The overall behavior along the trajectories of [Arg[91], Ala[96]] MBP$_{87–99}$ for the unrestrained (I) and backbone restrained MD runs (II and III) is analyzed. The following analysis focuses on the conformations with the lower energies ($\leq$6 kcal/mol from the lowest energy calculated conformations), that satisfy a set of criteria: (a) all backbone φ and ψ dihedral angles should occupy allowed regions of the Ramachandran map, and (b) all backbone ω dihedrals should be *trans*. Particular attention is given to explore the flexibility of the side chains [41].

3.4. Global behavior of [Arg[91], Ala[96]] MBP$_{87–99}$ in the MD trajectories

3.4.1. Trajectory I

The heavy-atom RMSD (in Å) for the selected 49 lowest energy structures was obtained as a function of time (Supplementary data). All these structures were acquired during the first 100 ps of the simulation. For the first 30 ps all the conformations retain a small RMSD, gradually increasing from 0.5 to 1 Å, followed by a change of about 1.3 Å for the next 10 ps. Relatively large conformational changes take place at 45 ps, varying from 1.8 till 2.3 Å for the following 20 ps. At 65 ps of run, a backbone dihedral conformation change occurs: a transition of the Phe[89] from the broad β minimum of the Ramachandran map to the lower left region. It is interesting to note that the central part of the molecule is similar in all conformations, while the NH and C termini present flexible molecular segments (Fig. 3a). The N-terminus is the most flexible segment, as superimposing the first four residues gives an RMSD of 3.82 Å Superimposing the last four amino acids in the C-terminus gives an RMSD of 2.83 Å.

3.4.2. Trajectories II–III

Dynamics run II, in which sequential $d_{\mathrm{NN}(i,i+1)}$ distance constraints were used, resulted in a set of very compact conformations, even after unrestrained minimization, which can not be justified by the NOE data, as long-range NOE connectivities were not observed. Thus, these structures were not further analyzed.

For run III, in which sequential $d_{\alpha\mathrm{N}(i,i+1)}$ distance constraints were used, the heavy-atom RMSD (in Å) for the selected 115 low energy structures was calculated as a function of time (Supplementary data). RMSD from the lowest energy conformation (Fig. 4a) ranges from 1.98 to 6.4 Å. Even though all selected conformations satisfy the criteria mentioned above, their RMSD when superimposing Cα, C, N, O, and Cβ is 3.327 Å, presenting conformational variation.

The lowest energy conformer obtained by dynamics has its φ and ψ backbone dihedral angles in the β region of the

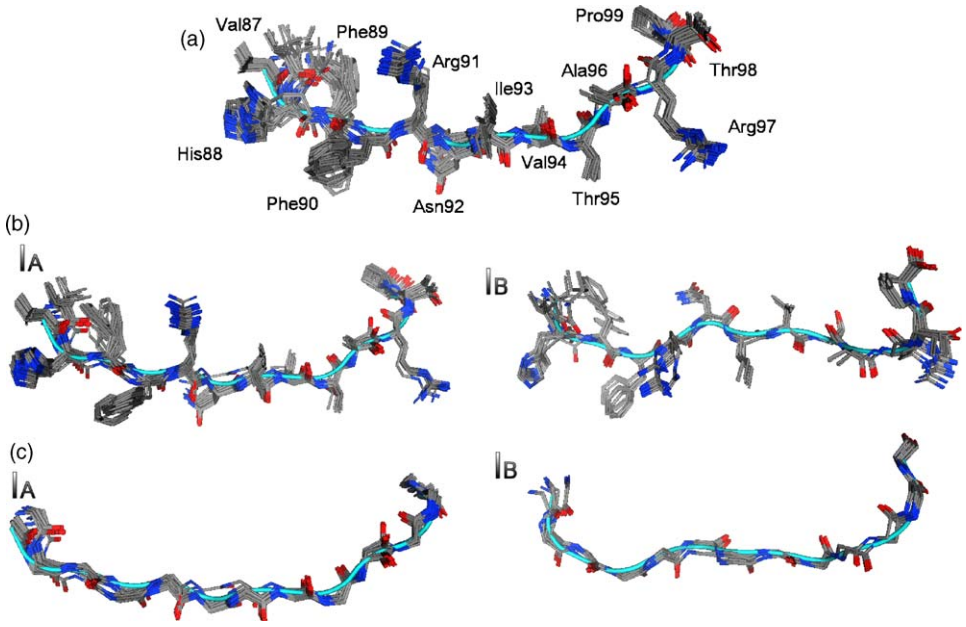

Fig. 3. (a) The ensemble of the conformers generated after applying unrestrained molecular dynamics to [Arg[91], Ala[96]] $MBP_{87–99}$, followed by energy minimization. (b) The two clusters (I_A and I_B) in which conformers were divided to, according to their backbone dihedral angles. (c) Backbone of all the conformations within I_A and I_B.

Ramachandran map. The middle part of the molecule forms a bend, but measured distances between amino acids Asn[92] to Val[94] are too long to characterize it as a turn. Change of RMSD is coupled with dihedral transitions for some amino acids to α_L or α_R conformations, and the transition of the π^*–π^* stacking of the Phe rings from a dihedral of -53° to a more edge-to-face orientation.

3.5. Backbone dihedral angles

The Ramachandran maps for all structures generated, are included in supplementary data.

3.5.1. Trajectory I

The 49 allowed lowest energy structures were clustered according to their backbone dihedral angles into two distinct groups I_A, and I_B (Fig. 3b and c). I_A is the set of conformations with their backbone angles occupying the β minimum of the Ramachandran map, whereas in I_B Phe[89] still belongs to the beta region, but is in the lower left region, with a negative ψ dihedral angle. The RMSD when superimposing Cα, Cβ, backbone C and backbone N heavy atoms for each cluster, is 0.84 and 0.79 Å, respectively.

A comparison of the backbone dihedrals of the lowest energy conformation of each cluster reveals that ψ of Val[87] changes from -40° in I_A to 126° in I_B, while in His[88] it changes from 95° to 80°, respectively. Main difference is for Phe[89]. φ and ψ shift from -120° and 165° in I_A to -145° and -150°, respectively in I_B. φ of Phe[90] is -155° in I_A and -140° in I_B, and ψ changes from 105° to 135°.

For residues Val[94] to Thr[98] φ of Thr[95] changes from about -60° to about -50°, while ψ of Ala[96] changes from 55° to about 110°. There is a major change in φ of Arg[97], which shifts from -80° to -140°. These backbone changes are responsible for the alteration of the side chain orientation. In I_A the specified part of the backbone forms a bend, and CO of Val[94] and Thr[95] point towards each other. The side chain of Val[94] is close to that of Ala[96], and the side chain of Thr[95] approaches Arg[97]. These spatial vicinities are not as evident in I_B.

Backbone NH–NH distances were also measured and compared with the ones obtained by NMR data (Table 3). The strong $d_{NN(96,97)}$ measured justifies the above spatial vicinities in cluster I_A, in contrast to the medium $d_{NN(96,97)}$ measured in cluster I_B. Lack of medium or strong $d_{NN(93,94)}$ connectivities agrees with the absence of the turn implied by the experimental distances for Asn[92]–Val[94].

3.5.2. Trajectory III

Unrestrained minimization following dynamics simulation III provided low energy conformations. Fig. 4b shows the lowest energy conformation of each of the eighteen clusters, derived after grouping them. Criteria for clustering were that (a) all conformers within each cluster should have dihedral angles that occupy the same region of the Ramachandran map, and that (b) RMSD of all structures within a cluster should present a deviation of less than 1 Å.

Conformers 8, 11, 12, 17, and 18 have some amino acids within the α_L minimum of the Ramachandran map, while in conformers 10 and 16 there are amino acids in both α_L and α_R minima. In clusters 2, 6, and 7 there are amino acids with backbone dihedral angles occupying the α_R minimum. All the rest have backbone angles occupying the β region, either in the broad region with positive ψ angle, or at the lower left region with negative ψ angle.

A superimposition of conformers 1–18, where backbone is represented as a cartoon, is presented in Fig. 5. As it can be

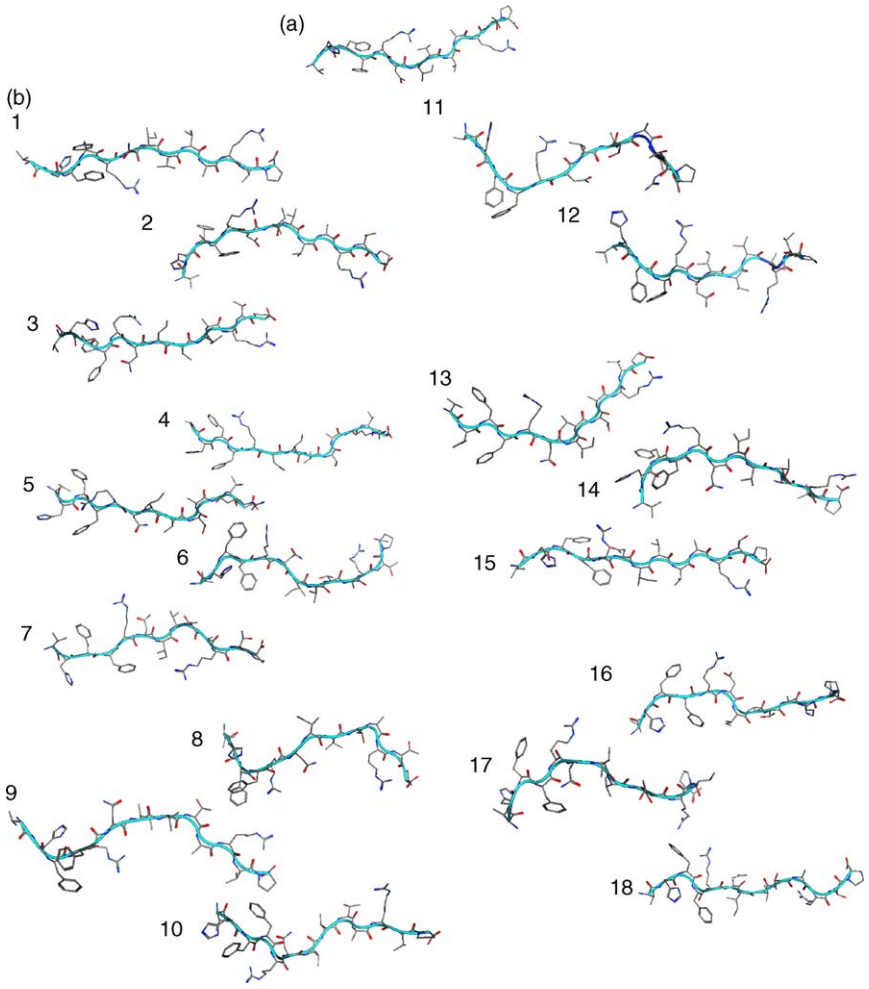

Fig. 4. (a) The lowest energy structure generated after applying backbone restrained molecular dynamics to [Arg^{91}, Ala^{96}] MBP$_{87–99}$, followed by unrestrained energy minimization. (b) The lowest energy structures of each of the eighteen clusters in which conformers were divided to, according to their backbone dihedral angles and their RMSD to the lowest energy conformation.

observed the NH and C termini occupy different spatial positions, depicting the molecule's high flexibility. All conformations adopt a general shape with a bend in the middle part of the molecule. The RMSD, though, when superimposing Cα, Cβ, backbone C, and backbone N heavy atoms is 3.53 Å, depicting backbone differences among the conformations.

Conformers 11 and 12 have an element of secondary structure identified: a 3-turn [42] between residues Ala^{96} and Thr^{98} (shown in blue in Fig. 5), with a hydrogen bond formed between the CO of Ala^{96} and the NH of Thr^{98}. This turn is due to residues 96 and 97 occupying the α_L region of the Ramachandran map, and is confirmed by $d_{NN(96,97)}$ and $d_{NN(97,98)}$, which for both clusters were found to be about 2.8 Å (Table 3). No such turn was identified for Asn^{92}–Val^{94} in any of the conformations, but medium $d_{NN(92,94)}$ and $d_{NN(93,94)}$ measured can explain the bends formed in 43% of the overall structures.

3.6. Flexibility of side chains—relative populations

To further examine inter atomic distances, histogram plots were obtained, to study the distribution of values. The values in each case were bucketed, and the number of counts per bucket was plotted. Values were normalized to correct for sample size and the results are displayed in percent. All histograms are included in supplementary data. Populations with inter atomic distances complying with NMR data were identified. Percentages mentioned refer to the overall number of the selected structures in each run.

3.6.1. Trajectory I

In Fig. 3b all conformations in the two clusters are presented. A close examination of the distance histograms, revealed some interesting features. The distances that were already estimated experimentally from our NMR data were measured, in order to check if the obtained conformations can be considered as present in the solution ensemble. All sequential Hα-NH distances comply with experimentally derived NOE connectivities. All $d_{\alpha N(i,i+1)}$ distances were found to be below 3 Å, except $d_{\alpha N(87,88)}$, which for 35% of the structures is about 3.5 Å.

The bend in the Asn^{92} to Val^{94} sequence, which was revealed by NMR calculated distances, is present in this ensemble of conformations, but distances are too long to allow the formation of a hydrogen bond; therefore, it cannot be classified as a turn.

Table 3
$d_{NN(i,i+1)}$ distances measured for different clusters obtained by both unrestrained (I_A and I_B) and backbone restrained (1–18) molecular dynamics

	$d_{NN(88,89)}$	$d_{NN(89,90)}$	$d_{NN(90,91)}$	$d_{NN(91,92)}$	$d_{NN(92,93)}$	$d_{NN(93,94)}$	$d_{NN(94,95)}$	$d_{NN(95,96)}$	$d_{NN(96,97)}$	$d_{NN(97,98)}$
I_A	W	W	M	W	S	W	W	W	S	W
I_B	M	M	M	W	S	W	M	W	M	M
1	W	W	M	W	W	M	W	W	M	W
2	W	W	W	M	W	W	W	M	M	M
3	W	W	M	M	W	W	W	W	M	W
4	M	M	W	W	W	W	M	W	M	W
5	M	W	W	M	M	W	M	W	M	W
6	W	W	W	W	W	W	M	M	M	W
7	M	W	W	W	W	M	M	W	W	M
8	W	S	S	W	W	W	W	W	M	M
9	W	W	M	W	W	W	M	W	M	W
10	W	S	M	S	W	W	W	M	M	W
11	W	W	W	W	W	W	M	M	S	S
12	W	W	M	M	W	W	M	M	S	S
13	W	W	M	W	W	M	W	M	M	W
14	M	W	W	M	M	M	W	M	M	W
15	W	W	W	M	W	M	W	M	M	W
16	W	W	W	W	M	M	M	M	M	W
17	W	M	M	W	W	M	W	M	W	W
18	W	M	W	W	M	M	W	W	W	S

S (strong) refers to distances smaller than 2.8 Å, M (medium) is used for distances from 2.8 to 3.8 Å, and W (weak) for distances ranging from 3.8 to 5.5 Å.

Most of the distances in the Val^{94} to Thr^{98} part of the molecule are in accordance with the medium range calculated NOEs, allowing these conformations to be included in those accepted as part of the ensemble in solution. A well-preserved spatial proximity is also that of Phe^{89} with Arg^{91}, in 84% of the conformations.

Flexibility is only observed in the first four amino acids. The NH terminus in 62% of the conformations is close to the ring of Phe^{89}, and in 57% it is near the ring of His^{88}. His^{88} approaches the ring of Phe^{89} as well, in 37% of the structures. The side chain of Phe^{89} moves towards the side chain of Phe^{90} in 27% of the selected structures, while in 27% of them it is relatively close to the side-chain of Asn^{92}. Asn^{92} in 41% of the structures is in the vicinity of Phe^{90}; this closeness is important for biological activity, as will be discussed later.

3.6.2. Trajectory III

Table 4 shows side chains' spatial proximities in each of the 18 clusters. As can be observed, all of them satisfy a range of the experimentally derived NOE distances and therefore all can be putative as present in the solution, in relative populations.

The NH terminus in 30% of the structures is close to the ring of Phe^{89}, while in 13% of them it approaches the ring of Phe^{90}. It also comes near the ring of His^{88} in 30% of the structures. The latter ring presents flexibility as well: in 17% of the overall number of conformers it is close to the ring of Phe^{89}, in 23% to that of Phe^{90}, and in 13% it moves towards side chain of Arg^{91}. Arg^{91} has two distinct orientations. In 57% of the structures its side chain is in spatial proximity with the ring of Phe^{89}, whereas in 40% of them it changes direction, towards side chain of Ile^{93}. Thirty percent of the conformations have the ring of Phe^{90} close to side chain of Asn^{92}, and a 43% form the bend in the middle part of the molecule designated by the Asn^{92}-Val^{94} NOEs. Ala^{96} in 30% of the structures is in vicinity with Val^{94}, while in 33% it is closer to Thr^{98}. Thr^{95} seems to favorably move towards Arg^{97}, since this distance is very small in 50% of the conformations, whereas in 27% it is closer to side chain of Ile^{93}.

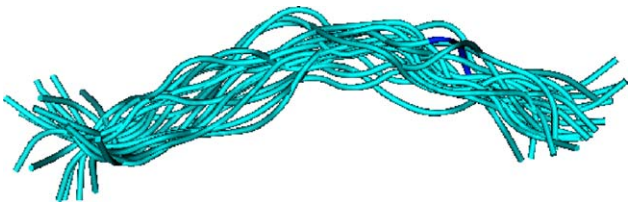

Fig. 5. The backbone of the ensemble derived after applying backbone restrained molecular dynamics to [Arg^{91}, Ala^{96}] MBP$_{87–99}$, followed by unrestrained energy minimization. Backbone is represented as a cartoon. Turns are indicated with blue.

It has to be noted that no single NOE contact is preserved across all clusters. This flexibility is justified by the amount of NOE peaks present in the NOESY spectrum acquired, which could not all be satisfied in a unique conformation. Individual populations that could not be identified by NMR solely due to their fast interconvention rate are spotted applying a combination of molecular dynamics and energy minimization. Theoretical methods rise as a solution for exploration of conformational space in the vicinity of conformers deduced from spectroscopic data. It has to be noted, though, that for system with large degrees of freedom dynamics may not identify all conformers in the conformational space. Indeed, unrestrained dynamics in this study did not identify all the various conformers dictated from NMR in the 1000 ps simulation time. Hence, its application in combination with experiment is essential.

3.7. Aromatic interactions

Aromatic-aromatic interactions are believed to form a fourth, and important class of possible interactions for amino acids in peptides, along with hydrogen bonds, electrostatics,

Table 4
Spatial proximity between side chains of amino acids, for the eighteen clusters derived after backbone restrained molecular dynamics

	Val^{87}–Phe^{89}	Val^{87}–Phe^{90}	Phe^{89}–Phe^{90}	Phe^{89}–Arg^{91}	Phe^{90}–Asn^{92}	Arg^{91}–Ile^{93}	Asn^{92}–Val^{94}	Ile^{93}–Thr^{95}	Val^{94}–Ala^{96}	Thr^{95}–Arg^{97}	Ala^{96}–Thr^{98}
1			*	*	*	*	*	*	*		*
2				*	*	*					*
3			*	*	*	*				*	
4	*			*					*		
5	*					*	*		*		
6		*		*						*	
7	*						*			*	*
8			*	*						*	
9			*			*			*	*	*
10		*		*	*				*	*	
11			*			*		*			*
12			*			*	*	*		*	*
13	*						*	*		*	*
14		*		*			*		*		*
15				*	*		*	*			*
16				*			*	*		*	
17		*		*	*	*	*	*		*	
18				*			*				*

(*): Indicates accordance with medium range NOE connectivities obtained from the NMR data.

and van der Waals interactions [43]. An interacting aromatic pair is defined as one for which the distance between phenyl ring centroids is less than 7 Å. For dynamics run I, no such interaction was identified, as the centroid separation for lowest energy structure from each cluster was 8.37 and 7.28 Å, respectively. For run III, though, a number of structures with interacting pairs were spotted (Fig. 6a). Out of the seven structures selected, only cluster 15 has a separation of 7.03 Å, while all the rest (clusters 1, 3, 8, 9, 11, and 12) have the most favored distance between rings of about 5 Å. Also, the lowest energy conformation has a centroid separation of 4.28 Å. A further examination of these structures was performed, regarding the orientation of the rings relative to each other.

To study the orientation of the rings, dihedral angles were measured (Fig. 6b). A perpendicular arrangement of aromatic rings, with dihedral angle $\pm 90^{\circ}$, is defined as an edge-to-face interaction [44]. All the above conformations adopt an approximate edge-to-face arrangement, with dihedrals ranging from -65° to -95°. The attractive electrostatic interaction between the rings contributes to a lower energy. The Phe rings of the lowest energy structure are orientated towards each other with a dihedral of -53°; in this conformational the arrangement of the planar surfaces leads to an increase in van der Waals contacts.

3.8. Proposed bioactive conformation of [Arg^{91}, Ala^{96}] $MBP_{87–99}$

MS is associated with MHC II molecules [45,46] (in human referred to as human leukocyte antigens (HLA)). The crystal structure of HLA-DR2b (DRA, DRB1*1501) was determined by Wucherpfennig et al. [47], complexed with $MBP_{85–99}$, a peptide from human MBP that was found to be immunodominant. In Caucasians, DRB*1501 is the most common DR2 haplotype. The natural ligand was isolated from the complex, and its conformation was used as a basis from which to establish criteria, in order to identify a putative bioactive conformation among all the low energy conformers that were generated for the APL [Arg^{91}, Ala^{96}] $MBP_{87–99}$. A putative bioactive conformation is defined in this study as one that theoretically exhibits optimal HLA binding affinity, having canonical MHC binding motifs, but fails to be recognized by the TCR and therefore to trigger an immune response. Thus, a set of criteria was used: (a) The structure should adopt a general backbone conformation very similar to that of the natural peptide, with an RMSD value of less than 2 Å when backbone Ca, C, and N atoms are superimposed; (b) distances between amino acids that serve as primary (Val^{87}, Phe^{89}) and as secondary anchors (Asn^{92}, Ile^{93}, and Thr^{95}) for binding to HLA-DR2b, should have a deviation smaller 20% when compared to the X-ray structure; and (c) in conformations that fulfill (a) and (b), residues that were previously found to be important for TCR recognition (His^{88}, Phe^{89}, and Lys^{91}) should be at a different position than on the natural peptide, and should present different spatial relations with the residues that bind to HLA-DR2b.

All the selected conformers generated by the dynamics simulations I and III were tested for compliance with the above criteria; the scan detected one single conformation that fulfills all of them (Table 5). RMSD of this conformation when superimposed to $MBP_{85–99}$ from the X-ray complex is 1.59 Å All the amino acids in this structure have their backbone dihedral angles within the β minimum of the Ramachandran map. Measured distance between the centroids of the Phe rings is 7.04 Å, just outside the cutoff value of 7 Å, and it cannot be classified as an interacting aromatic pair. The side chains' arrangement reveals a spatial proximity of Phe^{89}–Arg^{91}, Phe^{90}–Asn^{92}, Asn^{92}–Val^{94}, Ile^{93}–Thr^{95}, and Ala^{96}–Thr^{98}. Therefore, side chain interactions that are largely populated, as resulting from the extended analysis of molecular dynamics trajectories, are in agreement with criteria for bioactivity.

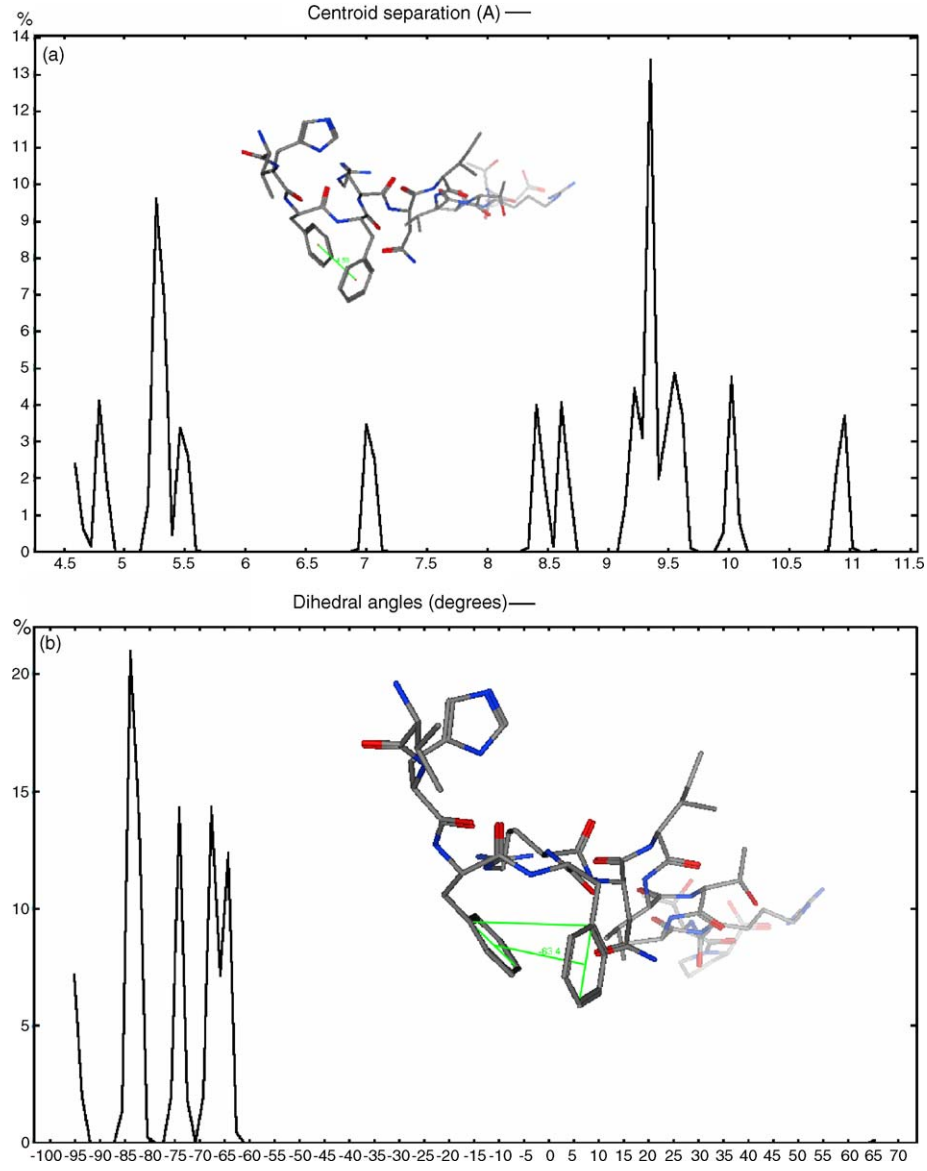

Fig. 6. (a) Centroid separation between rings of Phe^{89} and Phe^{90}, for the lowest energy conformations of each of the eighteen clusters, for backbone restrained molecular dynamics. Conformations with distance <7 Å are distinguished. (b) Dihedral angles of selected conformations from (a), showing the orientation of the rings. They all adopt an approximate edge-to-face interaction, with dihedrals approaching −90°.

In Fig. 7 [Arg^{91}, Ala^{96}] MBP$_{87–99}$ is superimposed with MBP$_{87–97}$ obtained from the crystal structure of the complex of MBP$_{85–99}$ with HLA-DR2b, after deleting the first two amino acids 85 and 86. The crystal coordinates were subjected to side-chain energy minimization, for removal of unfavorable atomic interactions. The C-terminus is different due to the replacement of Pro^{96} in the native peptide with an Ala in the APL. As can be

Table 5
Distances (in Å) between residues that serve as primary (Val^{87}, Phe^{90}) and secondary (Asn^{92}, Ile^{93}, Thr^{95}) anchors for MHC binding, for MBP$_{85–99}$ obtained from the crystal structure with PDB identity 1bx2, and linear antagonist [Arg^{91}, Ala^{96}] MBP$_{87–99}$

	MBP$_{85–99}$	[Arg^{91}, Ala^{96}] MBP$_{87–99}$
CG1(Val^{87})–CD1(Phe^{90})	11.54	10.6
CD2(Phe^{90})–OD1(Asn^{92})	4.85	3.59
CE2(Phe^{90})–CG2(Ile^{93})	6.59	5.53
CE2(Phe^{90})–CG2(Thr^{95})	10.54	10.09

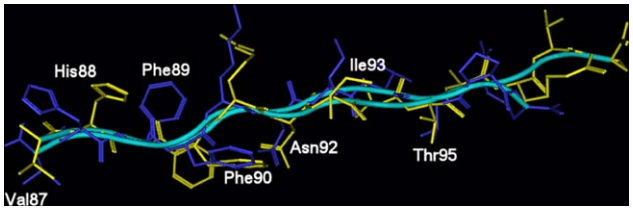

Fig. 7. Superimposition between MBP$_{87–97}$ obtained from the crystal structure of the complex with HLA (blue) and the proposed bioactive conformation of [Arg^{91}, Ala^{96}] MBP$_{87–99}$ (yellow). It is evident that primary MHC anchors (Val^{87}, Phe^{90}) and secondary MHC anchors (Asn^{92}, Ile^{93}, Thr^{95}) occupy the same region in space, whereas TCR contacts (His^{88}, Phe^{89}) have different orientation between the two structures.

observed the backbone of the N-terminus is almost identical. This is very important because it is known that the N-terminus is important for binding [48]. MHC contacts lie within the same region in space. Phe^{90} has the correct orientation to occupy the large hydrophobic pocket in HLA, whereas TCR contact Phe^{89} is no longer prominent and solvent exposed. Therefore, it is not accessible for interaction with the TCR.

The combination of NMR and MD studies led to a proposed bioactive conformation of the synthetic APL analogue that when superimposed to $MBP_{87–99}$ of the complexed $MBP_{85–99}$ obtained by crystallography with a 2.6 Å resolution, presents a striking similarity in the peptide binding sequence (backbone RMSD 1.23 Å). Thus, this approach rises as a valuable tool in the rational design of molecules with desired biologic activity.

4. Conclusion

Molecular dynamics calculation in combination with NMR structure determination is used to search the conformational space for structures that fulfill the experimental distance restraints. In our study both approaches were tried, in an attempt to generate as many of the distinct populations of conformations present in the solution as possible. Indeed, a bundle of conformers that are in accordance with the most critical NOEs were obtained, representing the true flexibility of the peptide. In particular, the molecule appears to have flexible termini segments and restricted motion in the central part. Medium intensity NOE peaks allow some secondary structure, i.e. the formation of bends and turns, but the side chain flexibility allows multiple contacts between the amino acids.

[Arg^{91}, Ala^{96}] $MBP_{87–99}$ is a peptide rationally designed to present antagonistic activity and the scope of this work was to correlate its activity with the 3D conformation it adopts. A set of criteria was established and all conformations generated were scanned. It was desired that HLA-DR2b contacts occupied the same region as in $MBP_{85–99}$ isolated from the crystal structure with the receptor, whereas amino acids serving as TCR anchors should have altered their orientation, preventing binding with the TCR. One structure matched the criteria, and is therefore proposed as the putative bioactive conformation. Interactions of the side chains that are largely populated in the conformational ensemble are present, accenting the combination of NMR and molecular dynamics as a valuable tool for the proposal of bioactive conformations.

Future work will include docking with the receptor followed by dynamics of the peptide-receptor complex, in order to obtain a refined preferable conformation that binds suitably to HLA-DR2b. The knowledge of the relationship of peptide conformation and antagonistic activity will lead to the rational design and synthesis of novel peptide analogues and ultimately peptide mimetic molecules for halting demyelination in MS.

Acknowledgment

Present work is supported by the Ministry of Development, Secretariat of Research and Technology of Greece (Grant EPAN YB/76).

Appendix A. Supplementary data

Supplementary data associated with this article can be found, in the online version, at doi:10.1016/j.jmgm.2005.09.010.

References

[1] S.J. Kenealy, M.A. Perical-Vance, J.L. Haines, The genetic epidemiology of MS, J. Neuroimmunol. 143 (2003) 7–12.
[2] E. Prat, R. Martin, The immunopathogenesis of MS, J. Rehab. Res. Devel. 39 (2002) 187–200.
[3] L. Barcellos, G. Thomson, Genetic analysis of MS in Europeans, J. Neuroimmunol. 143 (2003) 1–6.
[4] P.A. Muraro, M. Vergelli, M. Kalbus, D.E. Banks, J. Nagle, L.R. Tranquill, G.T. Nepom, W.E. Biddison, H.F. McFarland, R. Martin, Immunodominance of a low-affinity major histocompatibility complex-binding myelin basic protein epitope in HLA-DR4 subjects is associated with a restricted T cell receptor repertoire, J. Clin. Invest. 100 (1997) 339–349.
[5] A. Fassas, V.K. Kimiskidis, Stem cell transplantation for MS: What is the evidence? Blood Rev. 17 (2003) 233–240.
[6] H. Openshaw, B.T. Lund, A. Kashyap, R. Atkinson, I. Sniecinski, L.P. Weiner, S. Forman, Peripheral blood stem cell transplantation in MS with busulfan and cyclophosphamide conditioning: report of toxicity and immunological monitoring, Biol. Blood Marrow Transpl. 6 (2000) 563–575.
[7] C.L. Karp, C.A. Biron, D.N. Irani, Interferon β in multiple sclerosis: is IL-12 suppression the key? Immunol. Today (2000).
[8] A.J. Coles, M. Wing, Pulsed monoclonal antibody treatment and autoimmune thyroid disease in MS, Lancet 354 (1999) 1691–1695.
[9] O. Neuhaus, S. Strasser-Fuchs, F. Fazekas, Statins as immunomodulators: comparison with interferon β in MS, Neurology 59 (2002) 990–997.
[10] R. Liblau, R. Tisch, N. Bercovici, H.O. McDevitt, Systemic antigen in the treatment of T cell mediated autoimmune diseases, Immunol. Today 18 (1997) 599–604.
[11] M. Vergelli, B. Hemmer, U. Utz, A. Vogt, M. Kalbus, L. Tranquill, P. Conlon, P. Ling, L. Steinman, H. McFarland, R. Martin, Differential activation of human autoreactive T cell clones by altered peptide ligands derived from $MBP_{87–99}$, Eur. J. Immunol. 26 (1996) 2624–2634.
[12] L.B. Nicholson, A. Murtaza, B.P. Hafler, A. Sette, V.K. Kuchroo, A T cell receptor antagonist peptide induces T cells that mediate bystander suppression and prevent autoimmune encephalomyelitis induced with multiple myelin antigens, Proc. Natl. Acad. Sci. USA 94 (1997) 9279–9284.
[13] S. Brocke, K. Gijbels, M. Allegretta, I. Ferber, C. Piercy, T. Blankenstein, R. Martin, U. Utz, N. Karin, D. Mitchell, T. Veromaa, A. Waisman, A. Gaur, P. Conlon, N. Ling, P.J. Fairchild, D.C. Wraith, A. O'Garra, C.G. Fathman, L. Steinman, Treatment of experimental encephalomyelitis with a peptide analogue of myelin basic protein, Nature 379 (1996) 343–346.
[14] D.E. Smilek, D.C. Wraith, S. Hodgkinson, S. Dwivedy, L. Steinman, H.O. McDevitt, Single amino acid change in a myelin basic protein peptide confers the capacity to prevent rather than induce experimental autoimmune encephalomyelitis, Proc. Natl. Acad. Sci. U.S.A. 88 (1991) 9633–9637.
[15] B. Bielekova, B. Goodwin, N. Richert, I. Cortese, T. Kondo, G. Afshar, B. Gran, J. Eaton, J. Antel, J.A. Frank, H.F. McFarland, R. Martin, Encephalitogenic potential of the myeling basic protein peptide (amino acids 83–99) in multiple sclerosis: results of a phase II clinical trial with an altered peptide ligand, Nat. Am. 6 (2000) 1167–1175.
[16] L. Kappos, G. Comi, H. Panitch, J. Oger, J. Antel, P. Conlon, L. Steinman, the APL in Relapsing MS Study Group, Induction of a non-encephalitogenic type 2 T helper-cell autoimmune response in MS after administration of an APL in a placebo-controlled, randomized phase II trial, Nat. Am. 6 (2000) 1176–1182.
[17] T. Tselios, I. Daliani, S. Deraos, S. Thymianou, E. Matsoukas, A. Troganis, I. Gerothanassis, A. Mouzaki, T. Mavromoustakos, L. Probert, J. Matsoukas, Treatment of experimental allergic encephalomyelitis (EAE) by a rationally designed cyclic analogue of myelin basic

protein (MBP) epitope 72–85, Bioorg. Med. Chem. Lett. 10 (2000) 2713–2717.
[18] T. Tselios, I. Daliani, L. Probert, S. Deraos, E. Matsoukas, E. Roy, J. Pires, G. Moore, J. Matsoukas, Treatment of experimental allergic encephalomyelitis induced by guinea pig myelin basic protein epitope 72–85 with a human $MBP_{87–99}$ analogue and effects of cyclic peptides, Bioorg. Med. Chem. 8 (2000) 1903–1909.
[19] A.B. Vogt, H. Kropshofer, H. Kalbacher, M. Kalbus, H.G. Rammensee, J.E. Coligan, R. Martin, Ligand motifs of HLA-DRB5*0101 and DRB1*1501 molecules delineated from self-peptides, J. Immunol. 153 (1994) 1665.
[20] L. Yili, L. Hongmin, R. Martin, R.A. Mariuzza, Structural basis for the binding of an immunodominant peptide from myelin basic proteinin different registers by two HLA-DR2 proteins, J. Mol. Biol. 304 (2000) 177–188.
[21] N. Karin, D.J. Mitchell, S. Brocke, N. Ling, L. Steinman, Reversal of experimental autoimmune encephalomyelitis by a soluble peptide variant of a myelin basic protein epitope: T cell receptor antagonism and reduction of interferon gamma and tumor necrosis factor alpha production, J. Exp. Med. 180 (6) (1994) 2227–2237.
[22] M. Rance, O.W. Sorensen, G. Bodenhausen, G. Wagner, R.R. Ernst, K. Wütrich, Improved spectral resolution in COSY proton NMR spectra of proteins via double quantum filtering, Biochem. Biophys. Res. Commun. 117 (1983) 479–485.
[23] W. Willker, D. Leibfritz, R. Kerssebaum, W. Bermel, Gradient selection in inverse heteronuclear spectroscopy, Magn. Reson. Chem. 31 (1993) 287–292.
[24] W. Willker, D. Leibfritz, R. Kerssebaum, W. Bermel, Magn. Reson. Chem. 31 (1993) 287–292.
[25] L. Braunschweiler, R.R. Ernst, Coherence transfer by isotropic mixing: application to proton correlation spectroscopy, J. Magn. Reson. 53 (1983) 521–528.
[26] J. Jeener, B.H. Meier, P. Bachmann, R.R. Ernst, Investigation of exhange processes by two-dimesional NMR spectrometry, J. Chem. Phys. 71 (1979) 4546–4553.
[27] Chemical Computing Group Inc. 1010. Sherbrooke Street W, Suite 910; Montreal, Que., Canada H3A 2R7
[28] W.D. Cornell, P. Cieplak, C.I. Bayly, I.R. Gould, K. Merz, D.M. Ferguson, D.C. Spellmeyer, T. Fox, J.W. Caldwell, P.A. Kollman, A second-generation force field for the simulation of proteins, nucleic acids, and organic molecules, J. Am. Chem. Soc. 117 (1995) 5179–5197.
[29] G.V. Nikiforovich, B.G. Vesterman, J. Betins, Combined use of spectroscopic and energy calculation methods for the determination of peptide conformation in solution, J. Biophys. Chem. 31 (1988) 101–106.
[30] B. Vesterman, J. Saulitis, J. Betins, E. Liepins, G.V. Nikiforovich, Dynamic space structure of the Leu-enkephalin molecule in DMSO solution, Biochim. Biophys. Acta 998 (1989) 204.
[31] L. Verlet, Computer experiments on classical fluids. I. Thermodynamical properties of Lennard-Jones molecules, Phys. Rev. 159 (1967) 98–103.
[32] A.G. Ashish, R. Kishore, Characterization of a novel type VII β-turn conformation for a bio-active tetrapeptide rigin, Eur. J. Biochem. 267 (2000) 1455–1463.
[33] G.N. Ramachandran, C. Ramakrishnan, V. Sasisekharan, Stereochemistry of polypeptide chain configuration, J. Mol. Biol. 7 (1963) 95.
[34] G.N. Ramachandran, V. Sasisekharan, Conformations of polypeptides and proteins, Adv. Protien Chem. 23 (1968) 283–437.
[35] C. Ramakrishnan, G.N. Ramachandran, Stereochemical criteria for polypeptide and protein chain conformations. Part II. Allowed conformations for a pair of peptide units, Biophys. J. 5 (1965) 909–933.
[36] R. Laskowski, M. McArthur, D. Moss, J. Thornton, PROCHECK: a program to check the stereochemical quality of protein structures, J. Appl. Cryst. 26 (1993) 283–291.
[37] J. Matsoukas, V. Apostolopoulos, H. Kalbacher, A.M. Papini, T. Tselios, K. Chatzantoni, T. Biagioli, F. Lolli, S. Deraos, P. Papathanassopoulos, A. Troganis, E. Mantzourani, T. Mavromoustakos, A. Mouzaki, Design and synthesis of a novel potent myelin basic protein epitope 87-99 cyclic analogue: enhanced stability and biological properties of mimics render them a potentially new class of immunomodulators, J. Med. Chem. 48 (5) (2005) 1470–1480.
[38] G. Fisher, Chemical aspects of peptide bond isomerization, Chem. Soc. Rev. (2000) 119–127.
[39] H.J. Dyson, P.E. Wright, Defining solution conformations of small linear peptides, Annu. Rev. Biophys. Biophys. Chem. 20 (1991) 519–538.
[40] P.E. Wright, H.J. Dyson, R.A. Lerner, The physical basis for induction of protein-reactive antipeptide antibodies, Biochemistry 27 (1998) 7167.
[41] O. Galzitskaya, A. Caflisch, Solution conformation of phakellistatin 8 investigated by molecular dynamics simulations, J. Mol. Graphics Modell. 17 (1999) 19–27.
[42] W. Kabsch, C. Sander, Dictionnary of protein secondary structure: pattern-recognition of hydrogen-bonded and geometrical features, Biopolymers 22 (1983) 2577–2637.
[43] S.K. Burley, G.A. Petsko, Aromatic-aromatic interaction: a mechanism of protein structure stabilization, Science 229 (1985) 23–28.
[44] C.A. Hunter, J.K.M. Sanders, The nature of {pi}–{pi} interactions, J. Am. Chem. Soc. 112 (1952) 5525.
[45] MHC sequence consortium, A. Coles, Complete sequence and gene map of a human MHC complex, Nature 401 (1999) 921.
[46] A. Compston, A. Coles, Multiple sclerosis, Lancet 359 (2002) 1221.
[47] K.J. Smith, J. Pyrdol, L. Gauthier, D.C. Wiley, K.W. Wucherpfennig, Crystal structure of HLA-DR2 (DRA*0101, DRB1*1501) complexed with a peptide from human myelin basic protein, J. Exp. Med. 188 (8) (1998) 1511.
[48] K. Gerritse, C. Deen, M. Fasbender, R. Ravid, W. Boersma, E. Claassen, The involvement of specific anti myelin basic protein antibody-forming cells in multiple sclerosis immunopathology, J. Neuroimmunol. 49 (1994) 153.